Investigation of High Sensitivity Piezoresistive Pressure Sensors for -0.5…+0.5 kPa

Mikhail Basov, *R&D Engineer*
Denis Prigodskiy, *R&D Engineer*

***Abstract*. The investigation of the pressure sensor chip's design developed for operation in ultralow differential pressure ranges has been conducted. The optimum geometry of a membrane has been defined using available technological resources. The pressure sensor chip with an area of 6.15x6.15 mm has an average sensitivity S of 34.5 mV/кPa/V at nonlinearity $2K_{NL}$ = 0.81 %FS and thermal hysteresis up to 0.6 %FS was created. Owing to the chip connection with stop elements, the burst pressure reaches 450 кPa.**

***Index Terms*—piezoresistive pressure sensor, high sensitivity, temperature error, high mechanical strength, technology upgrading.**

I. Introduction

One of the most important directions of MEMS pressure sensors development is realization of silicon sensing elements able to work in ultralow pressure ranges of 0.1 to 1.0 kPa. Such pressure sensors may find application in many large-scale production fields (medicine, automotive industry, HVAC) and highly specialized scientific developments (seismology, biophysics, robotics) [1]. The opposite side of the task of achieving high piezosensitivity has been and remains an intent to reduce dimensions of a chip and, as a consequence, the package size of MEMS pressure sensors [2,3]. We can minimize the area of a chip by reducing sensitivity, while maintaining the principle of its mechanical design [4]. There are alternative methods for enhancing piezosensitivity or reducing chip dimensions that are associated with the application of a novel electric circuit PDA [5-8] using BJT. The development of such pressure sensors is still at the beginning of the road, but they have already demonstrated an obvious advantage over those with a classical Wheatstone bridge.

Simulated and experimental data on the proposed type of an ultrahigh sensitivity chip of a pressure sensor with a piezoresistive bridge circuit will be presented in the course of the work. In comparison with known analogs, the used chip structure has both strengths and weaknesses [9-13], but the criticality of its parametric values of output characteristics is heavily dependent on the application area of the sensing element.

This work was supported by the Dukhov All-Russia Research Institute of Automatics (VNIIA). (Corresponding author: Mikhail Basov.)

M. Basov and D. Prigodskiy are with VNIIA, Moscow 127055, Russian Federation (e-mail: engineerbasovm@gmail.com).

II. Modeling

A mathematical model of a pressure sensor chip operating in a range of 0.5 to 0.5 кPa is based on analytical and computer-aided calculation for trade-off relationship between sensitivity (required: S > 30.0 mV/kPa/V) and a nonlinearity error (required: $2K_{NL}$ < 1.5 %FS). The mechanical part of the sensing element includes a membrane with three separate and two bonded with the chip frame concentrators of mechanical stresses (MS), or rigid islands (RIs), where the thickness of RIs is equal to the initial thickness of a wafer. The selected structure of a membrane with RIs allows concentrating high MS at small values of deflection, which reduces a nonlinearity error [4, 14]. The geometrical shape of the membrane depends on the method of anisotropic wet etching that requires the expansion of the chip area due to silicon etching at an angle of 54.7°. For these types of ultrahigh sensitivity pressure sensor chips reactive ion etching (RIE) is frequently used, which significantly saves the area of a chip [15-20]. Figure 1 shows the geometrical parameters of the selected structure of a chip: L – length of a chip side, W – thickness of the membrane thinned part, H – chip thickness, A – area of the membrane thinned part, D – width of a gap between RIs, Z – length of a RI edge, Y – width of the chip frame, G – width of the membrane etch taper projection, Q_1 – distance between meddle piezoresistors (PRs), Q_2 – distance between end PRs. PRs of p-type, covering an area of 20x400 μm, are made on a silicon substrate of n-type ($N_C = 9\cdot10^{14}$ cm^{-3}) with a crystallographic plane (100) along the crystallographic direction [110] and have the following parameters: surface concentration $N_{Sp-} = 5.5\cdot10^{18}$ cm^{-3}, surface resistance R_{Sp-} = 200 Ohm/cm^{-2}, depth of a p-n junction x_{jp-} = 2.5 μm. The main piezoresistive coefficient is $\pi_{44} = 1.26\cdot10^{-9}$·Pa^{-1} at room temperature [21, 22]. The calculation of a change in PR rating and, consequently, output sensitivity and nonlinearity is performed using the theory of piezoresistive effect from the following formulas:

$$R_i(\Delta P) = \left(1 + \frac{1}{2}\cdot\pi_{44}\cdot\sigma(\Delta P)\right)\cdot R_{i0}, \quad (1)$$

$$\Delta V_{out}(\Delta P) = \frac{(R_1(\Delta P))\cdot(R_3(\Delta P)) - (R_2(\Delta P))\cdot(R_4(\Delta P))}{(R_1(\Delta P) + R_2(\Delta P))\cdot(R_3(\Delta P) + R_4(\Delta P))}V_{in}, \quad (2)$$

$$S = \frac{\Delta V_{out}(\Delta P)}{V_{in}\cdot\Delta P}, \quad (3)$$

$$2K_{NL_j}(\Delta P) = \frac{\Delta V_{out}(\Delta P) - \frac{\Delta V_{out}(0{,}5\ kPa) - V_0}{0{,}5\ kPa}\cdot\Delta P}{\Delta V_{out}(0{,}5\ kPa)}\cdot 100\%. \quad (4)$$

where ΔP –applied pressure rating, R_i (ΔP) and R_{i0} – PR rating (i = 1, 2, 3, 4) when ΔP is applied/ not applied, respectively; π_{44} – main piezoresistive coefficient for PR; σ(ΔP) – MS rat-

ing at ΔP; $\Delta V_{out}(\Delta P)$ – output signal of a bridge circuit at ΔP; V_{in} – bridge circuit supply voltage (5 V); S – sensitivity; $2K_{NL}$ –output signal nonlinearity error; V_0 – output signal at ΔP = 0.0 κPa; ΔV_{out}(0.5 kPa) – output signal at ΔP = 0.5 κPa. Table I provides geometrical parameters of the structure defined in the process of their variation. Figure 2 shows maps of mechanical stresses and the membrane deflection at ΔP = 0.5 κPa. Figure 3 shows the dependence of sensitivity and nonlinearity on the applied pressure for three thicknesses of the membrane (membrane geometry parameter with the highest dependence). Theoretical values of the output characteristics for the optimum thickness of the membrane (W = 8 μm) are S_{model} = 34.0 mV/κPa/V and $2K_{NLmodel}$= 0.68 %FS.

The analysis of possible deformation/deflection of the membrane resulted in determination of the required distances for free movement of the sensing element mechanical structure up to the stops (elements of a silicon assembly), needed to raise, in the operating pressure range, the threshold of burst pressure from both sides of the chip (required: P_{burst} > 300 κPa) [23, 24]. The deflection of the membrane at the rated voltage is $\Delta h_{0,5}$ = 2.7 μm. The bottom stop is made as an intermediate element between the chip and the base; it is bonded across the area of the chip frame and has via holes to apply pressure from the base. The top stop has a shape of a regular parallelepiped and is bonded from both sides of the chip, where there are no metallic pads; it also has unbonded regions to apply pressure from the topside of the chip (Figure 4). The gap $h_{touch\ model}$ = 5...23 μm between the chip membrane and the bottom and top stops is ensured by the thickness of a low-temperature bonding glass. The gap may vary to let the membrane move freely in the range of the rated pressure and have a margin up to the point close to destruction [25, 26]. That means that touching should occur at $P_{touch\ model}$ = 1.0…4.5 κPa. If the applied pressure exceeds the rated values, the chip membrane (before the moment it breaks) touches the stop and the area with a surface-to-surface contact is reallocated, which stops MS growth.

III. Technology

The main process steps of fabrication of pressure sensor ultrahigh sensitivity chips (Figure 5 and Table II) include:

1. Wafer thermal oxidation;
2. Sequence of micro cycles consisting of photolithography and follow-up doping of impurity of;
   a. Boron for high-alloy conducting areas of resistors (p^+-type);
   b. Boron for low-alloy areas of resistors (p^--type);
   c. Phosphorus for a substrate contact (n^+-type).
3. Si_3N_4 (PECVD) deposition as protection at membrane wet etching;
4. Membrane photolithography on the backside of a wafer (RIE);
5. Anisotropic wet etching of a membrane in 30% solution of potassium hydroxide at a temperature of 85 °C;
6. Anisotropic wet etching in $HF:HNO_3:CH_3COOH$ solution (2:9:4);
7. Si_3N_4 removal;
8. Photolithography of contact windows;
9. Sputtering of Al-Si (1.5 %) W_{Al-Si} = 0,8 μm;
10. Photolithography on metal surface;
11. Wafer dicing.

Technological processes of formation chip's top side guaranteed a spread in surface resistance R_S and, consequently, resistor rating (R_{bridge} = 4.5 κOhm) within 7% error and the presence of leakage current I_{leak} on p-n junctions of no more than 0.5 μA at room temperature at a reverse bias U_{sample} = 70 V. At anisotropic wet etching without self-hardening a spread in the membrane thickness was ΔW = ± 3 μm over 5 plates 100 mm in diameter. Besides large deviations of the membrane thickness from the required rated value W = 8 μm, we also observe asymmetry in the layout of RI edges due to a possible error of alignment at photolithography relative to a primary flat of the wafer and the use of silicon wafers with significantly misorientation crystallographic plane and primary flat (Figure 6a) [27, 28]. This deficiency substantially increases a nonlinearity error as the resistor body (p^--type) asymmetrically protrudes beyond the length of a RI edge. The further analysis of the obtained assemblies of pressure sensor chips, presented in the section below, showed that there was a difference in the rated values of sensitivity and nonlinearity, when applying pressure from the chip topside and backside, that was quite noticeable at W < 7 μm. Residual MS (compressive stresses) in chip structures are caused by the presence on the thinned part of the membrane of a step structure of SiO_2 (W_{SiO2} = 0.2…0.6 μm) resulted from diffusion and oxidation processes for different types of doped regions. The elimination of the deficiencies detected for these types of ultrahigh sensitivity chips [29-38] will allow in the future both to increase the percent yield and improve output characteristics within the stated requirements. For the purpose of testing, ultrahigh sensitivity chips of pressure sensors were first combined in a silicon assembly, comprising top and bottom stops and a base with low-temperature bonding glass between them (Figure 4). Connection with the selected geometry makes it possible not only to increase burst pressure of the sensor but also to reduce thermo-mechanical effect of the package [39-41]. The silicon assembly is connected to the package using silicon glue, the chip is wire to the package pins with the help of an aluminum wire (Figure 6b).

IV. Output Characteristics

Prior to testing, all samples of pressure sensors are subjected to thermo- and barocycling in order to remove residual MS from chip bonding. The studies were carried out at the circuit supply voltage V_{in} of 5.0 V for differential pressure in a range of -0.5 to + 0.5 κPa, with the element topside upwards. The primary parameters for ultrahigh sensitivity chips are sensitivity and nonlinearity that are to be measured at voltage supply from either side because of a certain asymmetry of the characteristics. The samples were divided in 3 groups with regard to the membrane thickness W: No.1 – 5…8 μm, No.2 – 8…9 μm, No.3 – 9…11 μm. Besides differences in the membrane thickness, there are spreads in the width of a gap between RIs

$\Delta D = \pm 3$ μm and the length of a RI edge $\Delta Z = \pm 60$ μm in each group of the samples.

The study of group No.3 is not relevant because of a low sensitivity S < 30 mV/κPa/V. Group No.1 with the required values of sensitivity showed that the application of these samples also lost its relevance due to a high nonlinearity error $2K_{NL}$ > 1.5 %FS. Group No.1 was divided into two subgroups based on the sensitivity rated values (No.1.1 – S ≈ 40…60 mV/κPa/V and No.1.2 – S ≈ 60…90 mV/κPa/V) in order to determine in further studies how greatly, relative to group No.2, an increase of sensitivity affects: 1) nonlinearity for this range, 2) zero signal $\Delta V_0(\sigma_r)$ due to residual MS from a SiO_2 layer. Figure 7 shows the output signal dependence on the applied pressure $\Delta V_{out}(\Delta P)$ for 10 average statistical samples in three types of groups. Table III contains the main output parameters; $\Delta V_0(\sigma_r)$ is calculated as follows:

$$\Delta V_0(\sigma_r) = \left(\frac{\Delta V_{out}(-0{,}1\ kPa) - \Delta V_{out}(+0{,}1\ kPa)}{2}\right) - V_0, \quad (5)$$

where ΔV_{out}(-0.1 kPa) – output signal at $\Delta P = 0.1$ κPa applied from the topside, ΔV_{out}(+0.1 kPa) – output signal at $\Delta P = 0.1$ κPa applied from the backside. Based on the analysis of $\Delta V_0(\sigma_r)$, it may be concluded that residual MSs from SiO_2 bend the thinned part of the membrane towards the topside of the chip, or upwards (Figure 4), which is more evident on subgroup No.1.2. In order to exclude the effect of MSs, arising from bonding the chip with the top stop by low-temperature glass, similar samples of subgroup No.1.2 were combined in an assembly without a top stop and demonstrated the identical bias effect of an output signal $\Delta V_0(\sigma_r)$. The observed effect that also manifests itself at a higher level of sensitivity, when pressure is applied from the topside, is kind of a "flap" of a thin stressed wafer. For elimination of the deficiency the process should be further modified to achieve the final trade-off relationship between MSs of different signs from SiO_2 and Si_3N_4 films [42-45]. Additional application of wet stop-etching and an increase in the length of a RI edge would make it possible not only to considerably reduce a spread in sensitivity, but to minimize the existing nonlinearity errors as well.

Table IV contains characteristics of group No.2 samples (62 samples) with an optimum membrane thickness W of 8 to 9 μm. The calculation of parameters as relative values associated with temperature characteristics, time stability and impact of overload pressure is carried out when pressure is applied from the membrane. Temperature parameters are measured in two separate temperature subranges: negative subrange from -30 °C to +20 °C, positive subrange from +20 °C to +60° C. Testing of mechanical strength is performed at an overload pressure P_{proof} of 30 κPa (pressure is applied from both sides of the chip). Time stability of an output signal was monitored within the first 9 hours after supplying power to the chip electric circuits. The effect of RI inertial mass at turning the chip by 180° was considered, which indirectly describes sensitivity of sensing elements, e.g., an accelerometer. With the analysis of output characteristics performed, it may be noted:

- Sensitivity and nonlinearity are differed rather insignificantly in measurements when pressure is applied from the topside or the backside. Average values of sensitivity and nonlinearity are S = 34.5 mV/κPa/V and $2K_{NL}$ = 0.81 %FS;
- Obtained errors TCZ < 0.1 %FS and TCS < 0.3 %FS, compensated by an external signal processing circuit (ASIC), are sufficiently acceptable;
- THZ and THS increase at positive temperatures as compared with negative temperatures. General values of temperature hysteresis are relatively low for this ultralow pressure range and do not exceed 0.6 %FS [46-48];
- Short-term time stability and signal variation due to the effect of mechanical overload are up to 0.3 %FS;
- A zero signal at turning the sensing element changes rather considerably, therefore the sensor can be used as accelerometer. On the other hand, this effect has a negative impact on its direct application as the crystal location and influence of the environmental vibration should be taken into consideration.

The selected structure of an assembly was analyzed with regard to free travel of the membrane of a chip of group No.2 up to the stops. As seen from Figure 8, the membrane travel remains free until the moment of touching $P_{touch\ samples}$ = 2…5 κPa, when pressure is applied from either side of the chip. These chip samples of group No.2 were tested for structure destruction in the absence of stops in the assembly. The membrane is irretrievably deformed at $P_{burst\ without\ stops} \approx 9$ κPa independently of the direction in which pressure is applied. When stops are used, the area of surface-to-surface contact between the membrane and stops is gradually reallocated at additional overload pressure and sensor is destroyed at a pressure above P_{burst} = 450 κPa.

V. Conclusion

Based on the developed mathematical model, the optimum geometry of a membrane structure has been defined and an ultrahigh sensitivity chip of a pressure sensor, operating in a ultralow differential pressure range of -0.5 to +0.5 κPa with S = 34.5 ± 4.1 mV/κPa/V and $2K_{NL}$ = 0.81 ± 0.50 %FS, has been realized. The difference in output characteristics measured when pressure is applied from the topside and the backside is relatively small (the difference in sensitivity is 2%) for the selected design of a chip. The samples show a certain spread in the rated values of sensitivity and sensor errors that can be minimized during further technological upgrading. The errors of temperature characteristics, time stability and overload ability of chips are also sufficiently small for the ultralow pressure range (Table 4). The RI inertial mass allows considering this chip as an ultrahigh sensitivity accelerometer. Additionally, an advantage has been achieved as the threshold of burst pressure P_{burst} was raised above 450 κPa owing to the use of stop elements in the assembly.

The presented structure of a pressure sensor may be valid for researches, involved in investigations in this field, from the viewpoint of further upgrade and fabrication of pressure sensors chips with ultrahigh sensitivity and low errors.

ACKNOWLEDGMENT

The studies were financially supported by Dukhov All-Russia Research Institute of Automatics.

REFERENCES

[1] https://www.i-micronews.com/bourns-expands-line-of-environmental-sensors-with-ultra-low-0-15-psi-pressure-sensor-models/

[2] https://www.i-micronews.com/nxp-s-multi-market-and-multi-technology-strategy-in-the-mems-pressure-sensor-business/

[3] L. Li, N. Belov, M. Klitzke, J-S. Park, High Performance Piezoresistive Low Pressure Sensors, IEEE Sensors Conference (2016) 1406-1408.

[4] S. Timoshenko, S. Woinowsky-Krieger, Theory of Plates and Shells, MCGraw-Hill, New York, 1970.

[5] M.V. Basov, D.M. Prigodskiy, Investigation of a Sensitive Element for the Pressure Sensor Based on a Bipolar Piezotransistor, Nano- and Microsystem Technology 19 (2017) 685-693.

[6] M.V. Basov, D.M. Prigodskiy, D.A. Holodkov, Modeling of Sensitive Element for Pressure Sensor Based on Bipolar Piezotransistor, Sensors and Systems 6 (2017) 17-24.

[7] M. Basov, Development of High-Sensitivity Pressure Sensor with On-chip Differential Transistor Amplifier, Journal of Micromechanics and Microengineering, 30 (2020) 065001.

[8] M. Basov, High-sensitivity MEMS pressure sensor utilizing bipolar junction transistor with temperature compensation, Sensors and Actuators A: Physical, 303 (2020) 111705.

[9] X. Huang, D. Zhang, A High Sensitivity and High Linearity Pressure Sensor Based on a Peninsulastructured Diaphragm for Low-Pressure Ranges, Sensors and Actuators A: Physical 216 (2014) 176-189.

[10] S. Marco, J. Samitier, O. Ruiz, J.R. Morante, J. Esteved, High-Performance Piezoresistive Pressure Sensors for Biomedical Applications Using Very Thin Structured Membranes, IOP Measurement Science and Technology 7 (1996) 1195-1203.

[11] Yu, Z., Zhao, Y., Sun, L., Tian, B., Jiang, Z., 2013. Incorporation of Beams into Bossed Diaphragm for a High Sensitivity and Overload Micro Pressure Sensor. Review Scientific Instruments. 84, 015004.

[12] A. Berns, U. Buder, E. Obermeier, A. Wolter, A. Leder, AeroMEMS sensor array for high-resolution wall pressure measurements, Sensors and Actuators A: Physical 132 (2006) 104-111.

[13] K.C. Katuri, S. Asrani, M.K. Ramasubramanian, Intraocular Pressure Monitoring Sensors, IEEE Sensors Journal 8 (2008) 12–19.

[14] N.S. Zemlyannikov, N.L. Danilova, V.V. Pankov, V.S. Sukhanov, Yu.A. Mikhailov, Tensoresistive Pressure Sensors on the Basis of Complex-Profled Silicon Membranes, Nano- and Microsystem Technology 4 (2013) 32-35.

[15] Tran, A.V., Zhang, X., Zhu, B., 2018. Mechanical Structural Design of a Piezoresistive Pressure Sensor for Low-Pressure Measurement: A Computational Analysis by Increases in the Sensor Sensitivity. Sensors. 18, 2023.

[16] Xu, T., Lu, D., Zhao, L., Jiang, Z., Wang., H., Guo, X., Li, Z., Zhou, X., Zhao, Y., 2017. Application and Optimization of Stiffness Abruption Structures for Pressure Sensors with High Sensitivity and Anti-Overload Ability. Sensors. 17, 1965.

[17] N. Arjunan, S. Thangavelu, Modeling and Analysis of a Multi Bossed Beam Membrane Sensor for Environmental Applications, Transactions on Electrical and Electronic Materials 18 (2017) 25–29.

[18] R.H. Johnson, S. Karbassi, U. Sridhar, B. Speldrich, A High-Sensitivity Ribbed and Bossed Pressure Transducer, Sensors and Actuators A: Physical 35 (1992) 93-99.

[19] A. Wu, J. Chen, X. Wang, A very sensitive pressure sensor on a SOI on cavity substrate, Proceedings of IEEE International SOI Conference (2007) 151–152

[20] C.T. Seo, Y.M. Kim, J.K. Shin, J.H. Lee, A Novel Comb-Type Differential Pressure Sensor with Silicon Beams Embedded in a Silicone Rubber Membrane, Jpn. J. Appl. Phys. 43 (2004) 2046–2049.

[21] Y. Kanda, A Graphical Representation of the Piezoresistance Coefficients in Silicon, IEEE Transactions on electron devices 29 (1982) 64-70.

[22] A.A. Barlian, W.T. Park, J.R. Mallon, A.J. Rastegar, B.L. Pruitt, Review: Semiconductor piezoresistance for microsystems, Proceedings of the IEEE, 97 (2009) 513–552.

[23] X. Huang, D. Zhang, Structured diaphragm with a centre boss and four peninsulas for high sensitivity and high linearity pressure sensors, Micro and Nano Letters 9 (2014) 460-463.

[24] Zhao, L., Xu, T., Hebibul, R., Jiang, Z., Ding, J., Peng, N., Guo, X., Xu, Y., Wang, H., Zhao, Y., 2016. A Bossed Diaphragm Piezoresistive Pressure Sensor with a Peninsula-Island Structure for the Ultra-Low-Pressure Range with High Sensitivity. IOP Measurement Science and Technology. 27, 124012.

[25] D.M. Prigodskiy, M.V. Basov, Research of Pressure Sensitive Elements with Increased Strength, Nano- and Microsystem Technology, Nano- and Microsystem Technology 6 (2019) 368-376.

[26] X.P. Wu, A New Pressure Sensor with Innercompensation for Nonlinearity and Protection to Overpressure, Sensors and Actuators A 21 (1990) 65-69.

[27] V. Lindroos, M. Tilli, A. Lehto, T. Motooka, Handbook of Silicon Based MEMS Materials and Technologies, William Andrew Applied Science Publishers, Oxford, 2010.

[28] J.C. Doll, B.L. Pruitt, Alternative Materials and Transduction Methods, in: Piezoresistor Design and Applications. Microsystems and Nanosystems, vol 1., Springer, New York, 2013.

[29] P.K. Guo, J. King, M. Lester, R. Craddock, A Hollow Stiffening Structure for Low-Pressure Sensors, Sensors and Actuators A: Physical 160 (2010) 35–41.

[30] Li, C., Cordovilla, F., Jagdheesh, R., Ocana, J.L., 2018. Design Optimization and Fabrication of a Novel Structural SOI Piezoresistive Pressure Sensor with High Accuracy. Sensors. 18, 439.

[31] P. Mackowiak, M. Schiffer, X. Xu, E. Obermeier, H. Ngo, Design and Simulation of Ultra High Sensitive Piezoresistive MEMS Sensor With Structured Membrane for Low Pressure Applications, 12th Electronics Packaging Technology Conference, (2010) 757-761.

[32] H. Sandmaier, K. Kuhl, A square-diaphragm piezoresistive pressure sensor with a rectangular central boss for low-pressure ranges, IEEE Transactions on Electron Devices 40 (1993) 1754-1759.

[33] A.A. Barlian, W.T. Park, J.R. Mallon, A.J. Rastegar, B.L. Pruitt, Review: Semiconductor piezoresistance for microsystems, Proceedings of the IEEE, 97 (2009) 513–552.

[34] M. Bao, L. Yu, Y. Wang, Micromachined beam-diaphragm structure improves performances of pressure transducer. Sensors and Actuators A: Physical 21 (1990) 137–141

[35] S. Armbruster, F. Schafer, G. Lammel, H. Artmann, C. Schelling, H. Benzel, S. Finkbeiner, F. Larmer, P. Ruther, O. Paul, A novel micromachining process for the fabrication of monocrystalline Si-membranes using porous silicon, The 12th International Conference on Solid-State Sensors, Actuators, and Microsystems (2003) 246–249.

[36] G. Lammel, S. Armbruster, C. Schelling, H. Benzel, J. Brasas, M. Illing, R. Gampp, V. Senz, F. Schafer, S. Finkbeiner, Next generation pressure sensors in surface micromachining technology, The 13th International Conference on Solid-State Sensors, Actuators, and Microsystems (2005) 35–36.

[37] B. Kloeck, S. D. Collins, N. F. de Rooij, R. L. Smith, Study of electrochemical etch-stop for high-precision thickness control of silicon membranes, IEEE Trans. Electron Devices 36 (1989) 663–669.

[38] K. Petersen, P. Barth, J. Poydock, J. Brown, J. J. Mallon, J. Bryzek, Silicon fusion bonding for pressure sensors, Tech. Digest 1988 IEEE Solid-State Sensor and Actuator Workshop (1988) 144–147.

[39] S. Guo, H. Eriksen, K. Childress, A. Fink, M. Hoffman, High temperature smart-cut SOI pressure sensor, Sensors and Actuators A: Physical 154 (2009) 255–260.

[40] D.M. Prigodskiy, M.V. Basov, Research of Pressure Sensitive Elements with Increased Strength, Nano- and Microsystem Technology, Nano- and Microsystem Technology 6 (2019) 368-376.

[41] X.P. Wu, A New Pressure Sensor with Innercompensation for Nonlinearity and Protection to Overpressure, Sensors and Actuators A 21 (1990) 65-69.

[42] A.V. Tran, X. Zhang, B. Zhu, Effects of temperature and residual stresses on the output characteristics of a piezoresistive pressure sensor, IEEE Access 7 (2019) 27668-27676.

[43] T. Guan, F. Yang, W. Wang, X. Huang, B. Jiang, D. Zhang, The Design and Analysis of Piezoresistive Shuriken-Structured Diaphragm Micro-Pressure Sensors, Journal of Microelectromechanical Systems PP(99) (2016) pp. 1-9.

[44] C. Iliescu, M. Avram, B. Chen, A. Popescu, V. Dumitrescu, D.P. Poenar, A. Sterian, D. Vrtacnik, S. Amon, P. Sterian, Residual stress in thin

films PECVD deposition: a review, Journal of Optoelectronics and Advanced Materials 4 (2011) 387-394.
[45] Nie, M., Bao, H., 2016. A theoretical model and analusis of composite membrane of a piezoresistive pressure sensor. AIP Advances. 6, 105302.
[46] Liu, Y., Wang, H., Zhao, W., Qin, H., Fang, X., 2016. Thermal-performance instability in piezoresistive sensors: Inducement and improvement. Sensors. 16, 1984.
[47] J.A. Chiou, S. Chen, Thermal hysteresis analysis of MEMS pressure sensors, Journal of Microelectromechanical Systems 14 (2005) 782-787.
[48] H.N. Chiang, T.L. Chou, C.T. Lin, K.N. Chiang, Investigation of the hysteresis phenomenon of a silicon-based piezoresistive pressure sensor, IEEE Conference International Microsystems, Packaging, Assembly and Circuits Technology (2007), 165-168.

Mikhail Basov was born in Domodedovo, Russian Federation, in 1989. He received the B.S. degrees in Nano- and Microelectronics engineering from the National Nuclear Research University "Moscow Physics Engineering Institute", in 2012.

Starting from 2010 he works as R&D engineer on advanced MEMS pressure sensing elements. His Ph.D. thesis is titled "High-Sensitivity Pressure Sensing Chip Utilizing Bipolar-Junction Transistors".

Denis M. Prigodskiy graduated from the National Research Technological University "MISIS", Moscow, Russia in 2008, in specialty microelectronics, engineer. He was a researcher at RPE "Kvant", Moscow from 2008 to 2012 and was engaged in heterostructural photoelectric solar cells for space applications. Since 2012, he has been working as a leading research engineer at the "All-Russian Research Institute of Automatics named after N.L. Dukhov", Moscow, and has been working on semiconductor devices and silicon-based pressure sensors. He is author and co-author of 10 publications and 4 patents in the field of semiconductor devices and MEMS technologies.

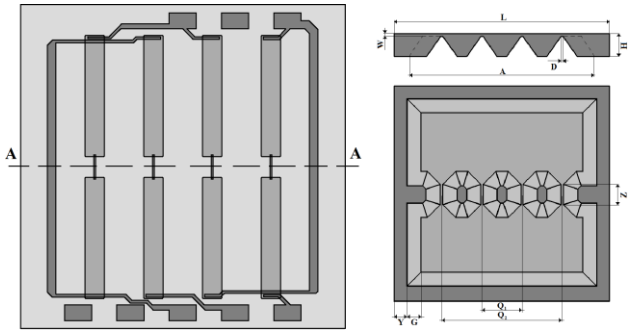

(a) (b)

Fig. 1. Schematic representation of an ultrahigh sensitivity pressure sensor chip: a) topside, b) backside

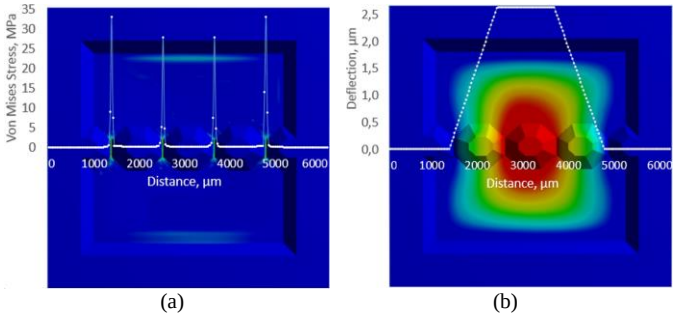

(a) (b)

Fig. 2. Map of MS distribution (a) and membrane deflection (b) for the selected membrane geometry at pressure 0.5 кPa

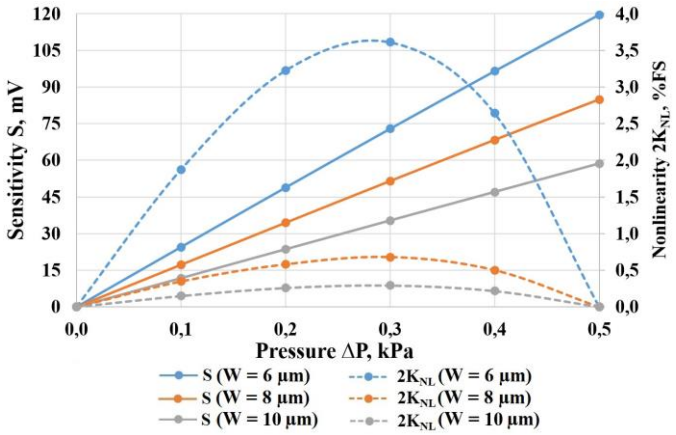

Fig. 3. Sensitivity (solid line) and nonlinearity (dot line) dependence on the pressure at variation of the membrane thickness W

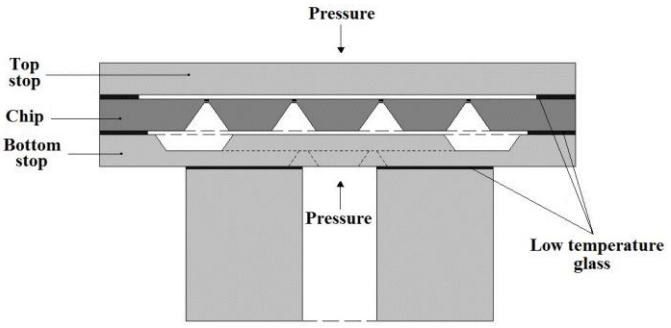

Fig. 4. Schematic representation of an assembly comprising a chip, stops and a base

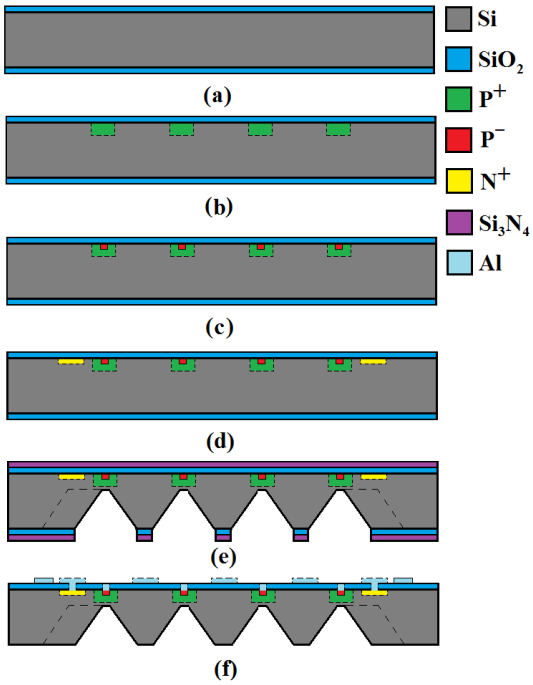

Fig. 5. Main process steps for an ultrahigh sensitivity pressure sensor chip (section A-A from Fig. 1)

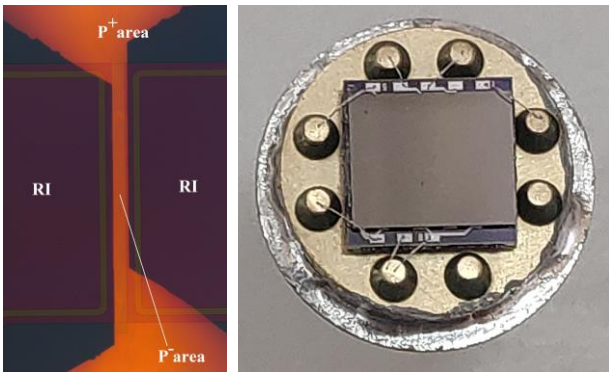

(a) (b)

Fig. 6. Examples of images of the obtained samples: a) rigid center geometry relative to PR regions, b) assembly in the package

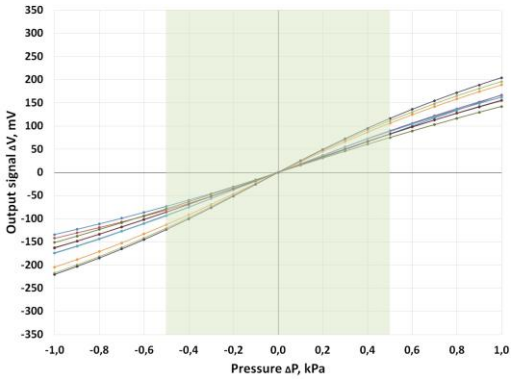

(a)

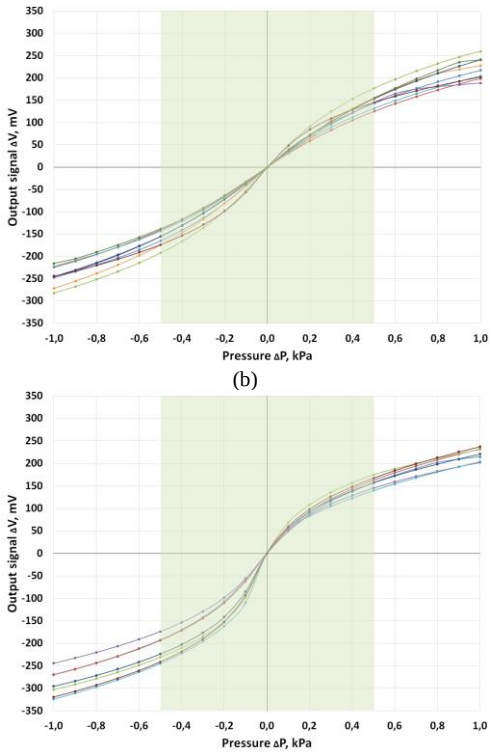

(b) (c)

Fig. 7. Variation of an output signal versus the applied pressure $\Delta V_{out}(\Delta P)$ for groups: a) No.2, b) No.1.1, c) No.1.2

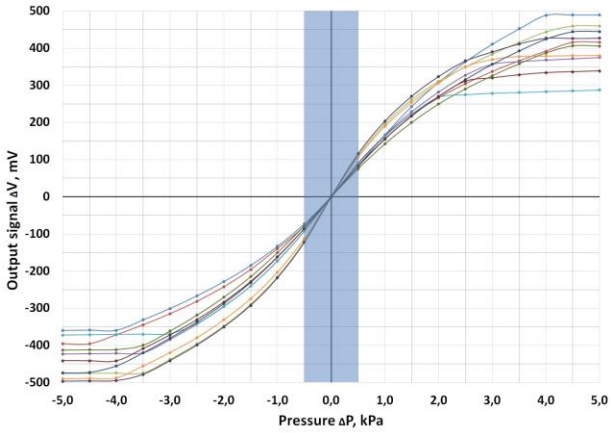

Fig. 8. Variation of an output signal versus the pressure for several typical samples of ultrahigh sensitivity pressure sensors

TABLE I
MAIN GEOMETRICAL PARAMETERS OF THE SENSING ELEMENT

Geometrical Parameter	Size, μm
L	6150
Q_1/Q_2	1122/3366
W	8
H	420
A	4200
D	18
Z	400
Y	690
G	285

TABLE II
DIFFUSION PARAMETERS OF ULTRA-HIGH-SENSITIVITY PRESSURE SENSOR

Process step	Parameters
Oxidation	1100 ºC, 15 min.-20 min.-15 min (dry-wet-dry)
Forming high-doped P^+ areas	Diffusion from unlimited source: 1050 ºC, 55 min. Drive-in and oxidation: 1150 ºC, 5 min – 15 min. – 5 min (dry-wet-dry)
Forming P^- resistors	Ion implantation: $D = 8.0 \cdot 10^{14}$ cm^{-2}, E = 50 keV Impurity activation and oxidation: 1100 ºC for 45 min in inert atmosphere followed by oxidation 1000 ºC, 5 min – 35 min. – 5 min. (dry-wet-dry)
Forming N^+ areas	Diffusion from unlimited source: 1000 ºC, 5+30+10 min. (Ar/O_2+Ar/O_2/$POCl_3$+Ar/O_2) Drive-in and oxidation: 1000 ºC, 5 min – 30 min. – 10 min (dry-wet-dry)

TABLE III
INFLUENCE OF TECHNOLOGICAL ERRORS

Parameters		Type of chip №2	№1.1	№1.2
Sensitivity S, mV/V/kPa	Backside	34,2 ± 3,9	49,2 ± 8,6	73,2 ± 12,9
	Topside	34,8 ± 4,2	50,5 ± 8,9	75,2 ± 14,0
Nonlinearity $2K_{NL}$, %FS	Backside	0,77 ± 0,48	3,5 ± 2,1	9,5 ± 2,9
	Topside	0,85 ± 0,52	4,5 ± 2,3	10,0 ± 3,2
$\Delta V_0(\sigma_r)$, mV		0,26 ± 0,26	1,61 ± 0,59	8,72 ± 6,22

TABLE IV
PERFORMANCE OF ULTRA-HIGH-SENSITIVITY PRESSURE SENSOR

Parameters		Value
Sensitivity S, mV/V/kPa	Backside	34,2 ± 3,9
	Topside	34,8 ± 4,2
Nonlinearity $2K_{NL}$, %FS	Backside	0,75 ± 0,48
	Topside	0,87 ± 0,52
Zero pressure output signal (Offset) V_0, mV/V		< 5
TCZ (–30…+20 °C), %FS/°C		0,055 ± 0,051
TCZ (+20…+60 °C), %FS/°C		0,048 ± 0,044
TCS (–30…+20 °C), %FS/°C		0,280 ± 0,021
TCS (+20…+60 °C), %FS/°C		0,234 ± 0,026
Zero thermal hysteresis (THZ)	(–30…+20°C), %FS	0,21 ± 0,13
	(+20…+60°C), %FS	0,34 ± 0,25
Span thermal hysteresis (THS)	(–30…+20°C), %FS	0,12 ± 0,11
	(+20…+60°C), %FS	0,21 ± 0,18
Long-term instability	of zero offset, %FS	0,18 ± 0,11
	of pressure sensitivity, %FS	0,10 ± 0,09
Burst pressure P_{burst}, kPa		> 450
Changing after proof pressure P_{proof}	zero, %FS	0,19 ± 0,11
	span, %FS	0,11 ± 0,08
Zero offset after turning on 180°, μV/V		52 ± 10
Number of samples in statistics		62